# Effect of lateral contraction and magnetism on the energy release upon fracture in metals: First-principles computational tensile tests

Z. X. Tian, J. X. Yan, W. Xiao, and W. T. Geng*
*School of Materials Science and Engineering, University of Science and Technology Beijing, Beijing 100083, China*
(Received 27 September 2008; revised manuscript received 29 January 2009; published 20 April 2009)

On many occasions, there is an energy release upon fracture of materials. Taking the Σ5 (210) grain boundary in nickel as an example, we have studied the effect of lateral contraction (the Poisson effect) upon stretching and the effect of magnetism on the energy release at the break point, using density-functional theory computational tensile tests. For both clean and sulfur segregated grain boundaries, our calculations show that the Poisson effect can reduce the total energy of the grain-boundary system remarkably. For Σ3 (111) grain boundary, however, lateral optimization of the computation cell has only a minor effect because of the close packing of the Ni (111) plane. Surprisingly, magnetism is found to reduce much of the energy release upon fracture for grain boundaries for such a weak magnetic metal. As a result, the calculated ultimate tensile strength of the material will be significantly diminished. Segregated sulfur atoms reduce the energy barrier between metastable and ground-state configurations in straining procedure. Near the break point, spin polarization of the interfacial atoms is significantly enhanced which introduces an extra energy lowering of the system.

DOI: 10.1103/PhysRevB.79.144114 PACS number(s): 61.72.Mm, 81.05.Bx, 68.35.Dv

## I. INTRODUCTION

Intergranular embrittlement induced by impurity segregation in a grain boundary (GB) has a direct effect on the mechanical properties of metallic materials.[1] A thermodynamic theory developed by Rice and Wang[2] describes the mechanism of the metalloid-induced intergranular embrittlement through the competition between plastic crack blunting and brittle boundary separation. According to this theory, the potency of a segregation impurity in reducing the "Griffith work" of a brittle boundary separation is a linear function of the difference in binding energies for that impurity at the GB and the free surface (FS). The first-principles calculations based on Rice-Wang model (FPRW) have been carried out in the last 20 years to evaluate the embrittling or strengthening effect of segregants on GB cohesion.[3–11] Fairly good agreement between theory and experiment has been obtained for many cases.[12] The attempt in electronic structure analysis in these investigations is to elucidate the binding-energy dependence of the segregant on its atomic structure difference between the initial (stress-free GB) and eventual (FS) states. With these quantitative studies, it becomes more and more clear how bonding characteristics and atomic size effect contribute to GB embrittlement or enhancement.[13–16]

On the other hand, with the aid of ever-growing computing power, it is now feasible to simulate vividly the fracture of a material along the GB. The mechanical effect of a GB segregant can be illustrated by the response of a GB with impurity segregation to a tensile or shear stress. Over a decade ago, Deyirmenjian *et al.*[17] performed first-principles tensile test for Al containing one-dimensional defects. The supercell used to model this system was extended by a small increment, and then all the atoms were allowed to fully relax using the first-principles pseudopotential method. They obtained the total energy and the average stress for each level of extension, and by iterating this cycle, observed failure from the weakest point at some critical stress. Using the same approach, Kohyama[18,19] investigated the Σ9 (122) tilt GB in cubic SiC with nonpolar and polar interfaces. He found that the atomic-scale inhomogeneity associated with the interfacial bonds seriously affects the tensile strength and interfacial fracture. More recently, Lu and co-workers[20–23] carried out a series of study on the mechanical behavior of Na, Ca, S, and Ga on the Σ9 (122) GB cohesion in Al. Through first-principles computational tensile test (FPCTT), changes in chemical bonding near and across the GB as a response to the applied stress demonstrate clearly how the GB cohesion is weakened by the segregated impurities. Their calculations showed the ultimate tensile stress (UTS) of Al containing a Σ9 (122) GB is always reduced if any of Na, Ca, S, or Ga segregate to the GB region and thus support experiment in that all these elements behave as GB embrittlers. Fracture occurs along the GB plane and is dominated by the break of the interfacial bonds.

Regarding the accuracy of the density-functional theory (DFT) computations, we want to mention that in a very recent study, Lee *et al.*[24] measured the elastic properties and intrinsic breaking strength of free-standing graphene monolayer by nanoindentation in an atomic force microscope. The UTS they obtained is $130 \pm 10$ GPa, which is excellent agreement with the simulated value (between 118 and 121 GPa) using first-principles methods.[25,26] This is strong evidence that the DFT is a powerful weapon in tackling difficult problems concerning mechanical properties of solids.

While FPRW demands total-energy calculations only for the initial and eventual configurations for a fracture along the GB, i.e., clean and impurity-segregated GBs, clean and impurity-adsorbed FSs, FPCTT necessitates a large number of intermediate stretching states.[27] Since we have to pay a high price in order to watch atomically and electronically the vivid picture of fracture, we are particularly more critical about the reliability of the output it yields. In practice, the impurity-induced GB embrittlement occurs in polycrystalline materials with a large amount of extensive defects.

 

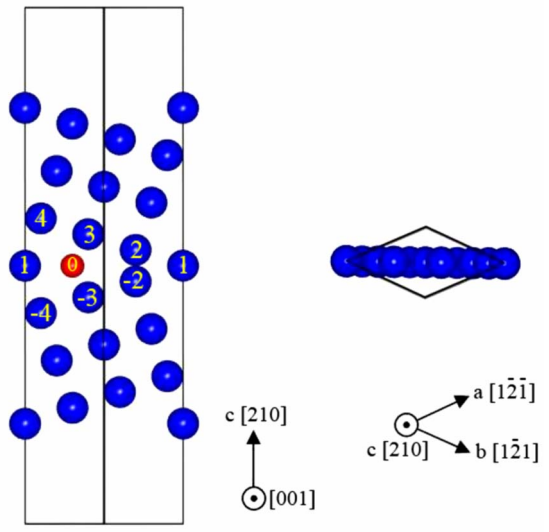


FIG. 1. (Color online) Side and top views of the computation cell used to model the Σ5 (210) [001] tilt GB in Ni. Atoms near the GB are numbered by the atomic layer counted from the GB plane. 0 denotes the interstitial site at the GB core.

Molecular-dynamics (MD) simulations of nanocrystalline metals have been carried out to help understanding the GB-related phenomena.[28–33] Many different stretching procedures have been used (with and without the Poisson effect) and have been thoroughly evaluated. Using *in situ* peak profile analysis, Budrovic *et al.*[32] studied the plastic deformation in nanocrystalline Ni GB with grain size of 30 nanometers, and the maximum strength in their results is about 2.25 GPa at a strain of 4%. In a very recent study, MD simulations on nanocrystalline Ni were carried out by Cao and Wei[33] using the embedded-atom method. Their simulation cell contains 18 grains with an average grain diameter of 12 nanometers. The maximum strength they obtained is 5.2 GPa at a strain of 4%. Note that these theoretical UTS, although greatly reduced by considering Poisson effect, are still much higher than the real materials in use. Such a huge discrepancy is generally ascribed to the existence of other kind of extensive defects like dislocations.

In first-principles computation, the target material is simplified to an ideal two-grain system (see Fig. 1 below). This is presumably the main reason that the computed UTS is (~10 GPa) even higher than MD results for nanocrystals and often dozens of times higher than the real metals in use (~1 GPa). Therefore, unlike the single-crystal cases such as monolayer graphite mentioned above,[24] quantitative comparison between computation and experiment has to be made with great care. Rather, the focus in scrutinizing the FPCTT method should be on the robustness of its results (e.g., UTS) with respect to the computation settings and parameters.

In all the above mentioned FPCTT work,[17–23] the initial atomic positions were obtained by enlarging the optimized computation cell in last strain step. That is, the system containing GB was viewed as a perfect crystal and the applied stress was assumed to impose on every atom instantly. In their attempts to understand the sulfur-induced GB embrittlement in nickel, Yamaguchi *et al.*[34–36] assumed *a priori* that fracture occurs at the GB plane and insert an incremental vacuum slab at the boundary for each strain step. This stretching scheme makes use of experimental evidence that fracture occurs along the GB which makes guess of atomic positions more reasonable. The drawback of such an option, nonetheless, is that it diminishes the power of prediction of FPCTT. Although different stretching procedures have been used and evaluated in molecular-dynamics works, as mentioned above, up to this date, no first-principles DFT works employing different stretching schemes on the same physical system and making comparison of them have been reported, to the best of our knowledge.

A more important issue in the FPCTT is the Poisson effect. To take the lateral (i.e., freedoms within the GB plane) contraction of the supercell during stretching into account, one has to optimize the atomic structure for every strain step, which means an increase in the computation effort by quite a few times. To make the simulation more affordable, the Poisson effect was neglected in the previous computational works reported in literature. Since it lowers the total energy for both clean and impurity segregated GB systems, the Poisson effect will in many cases not affect the predicted mechanical behavior of the segregant, i.e., either strengthening or weakening the cohesion across the GB. To achieve more precise FPCTT, nevertheless, it is desirable to evaluate the numerical error induced by neglecting lateral contraction in the stretching the material.

In addition, the interfacial atoms experience abrupt loses of nearest neighbors at the break point. For magnetic (Fe, Co, and Ni) transition metals, a reduced coordination number (e.g., from three dimensions to two or one dimension) usually means an enhanced spin polarization; and even for a number of nonmagnetic transition metals, magnetism appears at surfaces.[37,38] In fact, our previous DFT investigation[39] on the magnetic properties of the clean and Li-, B-, P-, and Ca-adsorbed Ni (210) surface demonstrated that there is a strengthening (diminishing) of surface magnetism for the clean (metalloid-adsorbed) surface. As a consequence, spin polarization might have a significant effect on the energy release upon rupture, which in turn influences the UTS of the system.

In this paper, we take the Ni Σ5 (210) GB system as an example to address the above issues. In addition to the aforementioned two stretching schemes, we propose a third scheme in which we always pull the two end layers of the slab to the expected eventual positions and then fully relax all the other atoms. Our detailed comparative study of these three distinct stretching schemes demonstrate that near the breaking point, the total energy of the computation cell as a function of strain varies with stretching schemes. In small strain region, on the other hand, they do match each other very well. As a result, the calculated UTS varies to some extent on how the material is being stretched. Interestingly, our laborious calculations involving the Poisson effect demonstrate clearly that all three total energy versus strain curves will merge into one for both clean and sulfur-segregated GB systems if the Poisson effect is taken into account. Our calculations on another GB, Σ3 (111) reveal a totally different result: the lateral optimization of the computation cell has only a negligible effect due to the close packing of the Ni

(111) plane. Unexpected for a weak magnetic metal, we find that magnetism reduces remarkably the energy release upon fracture along the GB in Ni. Accordingly, the calculated UTS of the GB system will suffer a decrease. The calculated electronic structure shows that upon fracture, the magnetic moments of the interfacial atoms are significantly boosted which favor the free-surface configuration and hence a reduced cohesion across the GB. The remainder of the paper is organized as follows. In Sec. II, we describe the model and computational details. Results and discussion are presented in Sec. III, and in Sec. IV we give a short summary.

## II. MODEL AND COMPUTATION

We have performed the first-principles DFT calculations using Vienna *ab initio* Simulation Package (VASP).[40] The electron-ion interaction was described using the projector augmented wave (PAW) method,[41,42] the exchange-correlation potential using the generalized gradient approximation (GGA) in the Perdew-Burke-Ernzerhof (PBE) form.[43] We used the same input parameters as in Refs. 34 and 35. The cut-off energy for the basis set was 280 eV. The Brillouin-zone integration was performed within Monkhorst-Pack scheme using a $(4\times4\times1)$ mesh and the Methfessel-Paxton smearing with a width of 0.1 eV. The energy relaxation for each strain step is continued until the forces on all the atoms are converged to less than $10^{-2}$ eV $Å^{-1}$.

We have modeled the $\Sigma5$ (210) [001] tilt GB in nickel using a supercell illustrated in Fig. 1. The atomic sites are labeled by numbers counted from the GB plane. One unit cell is composed of two identical grains (each contains 11 atomic layers with one in common), which form a tilt GB in between. Test calculations on a unit cell containing 41 atoms have been done [see the end of Sec. III-(i)] There is one atom in one Ni (210) layer. Since we have used a periodic boundary condition, we separate the neighboring slabs in [210] direction by a vacuum region of about 10 Å to minimize the interaction between slabs. The two-dimensional lattice constant for stress-free systems was chosen to be that of the bulk value for fcc Ni, 3.52 Å, that was also reproduced in our GGA-PBE computation. The (210) interlayer distance for the ideal system is therefore 0.79 Å. Site 0 denotes the core of GB free volume around which impurity atoms can reside. We note that when one S atom is put into GB(0) or GB(2) site, we are in fact introducing a full monolayer of S onto the GB. This is obviously a very high impurity concentration, yet not so much unrealistic.[44] Previous density-functional theory computation[34,35] on 1/4, 2/4, 3/4, and 4/4 S layer (no lateral optimization and no spin polarization) demonstrated progressive embrittling effect of S. Thus, discussion on segregation of one monolayer of S is meaningful in FPCTT.

## III. RESULTS AND DISCUSSION

### A. Stretching without lateral optimization

To embark on the FPCTT, one has first to determine the positioning of sulfur in the nickel matrix, with and without applied stress. In the absence of applied stress, Yamaguchi *et al.*[34,36] already showed and Geng *et al.*[35] confirmed that the sites GB(2) and GB(0) have over one eV stronger binding for sulfur atom than other positions. This result is reproduced in the present work. In a famous work, Shinoda and Nakamura[45] discovered that segregation of phosphorus segregation at the GB in steel was enhanced by tensile stress and lessened by compressive stress, but after stress aging, the accumulation or depletion would disappear. Such a nonequilibrium GB segregation will probably also take place in the S/Ni case discussed here. However, the segregation process typically takes hours or even days, much longer than the time for a tensile test.[44] Therefore, the distribution of sulfur near the GB will be nearly the same as in the relaxed case when the material breaks. In other words, the sulfur atoms are very unlikely to exchange positions with neighboring nickel atoms. In view of this fact, we will not consider sulfur segregation in the stretching process and will keep them in GB(2) or GB(0) sites.

In the most commonly used stretching method, one sets the starting atomic configuration in each strain step by elongating uniformly the fully relaxed configuration of the preceding step.[17–23] In doing so, we can ensure steady movements of atoms. In the second stretching process that was utilized by Yamaguchi *et al.*,[34] the GB plane is set *a priori* as the fracture plane and the upper and lower half of the crystal blocks is put away from each other gradually. And in the stretching process III, we stretch the two end layers of the unit cell to the expected scale and fixed them. In the latter methods, stretching is respect to the initial configuration in each step, and then we relax all the other atoms.

We show in Fig. 2 the calculated total binding energy of the clean Ni $\Sigma5$ (210) GB system (panel a) and that with a S atom segregated to the interstitial GB(0) (panel b) or substitutional GB(2) (panel c) positions. The valence electron densities in the (001) plane are plotted in Fig. 3 for a few representative strain steps for each system. It is seen clearly in Fig. 2 that for all three systems, the energy-versus-strain curves and figures have very similar values and structures for stretching schemes I, II, and III in the low strain region. As the system is further stretched up to the fracture point, nevertheless, the three curves are separated from each other in panels (a) and (b). For the clean GB without S segregation, the first and the third stretching approaches failed to separate the two grains even with a strain as large as 30%, whereas process II succeeded. The main reason for this failure is that a tilt GB has reflection symmetry along the stress direction. In such a case, the atoms at GB core may have metastable state when stretched. To verify such an explanation, we have reoptimized the geometries for the points that have a total binding energy higher than that after the fracture, moving by hand the GB core atom to one side of the cell and hence seriously broke the vertical symmetry of the two grains. It turned out that we can always break the GB by such a strong perturbation.

Another reason for the failure of processes I and III to break the GB is the strong chemical bonding across the boundary plane. In the absence of external stress, the GB(3)-GB(−3) bond are longer and the GB(2)-GB(−2) bond are shorter than the equilibrium Ni-Ni nearest-neighbor distance in a perfect bulk environment, thus the chemical interaction in both of them is weaker than in a normal Ni-Ni bond

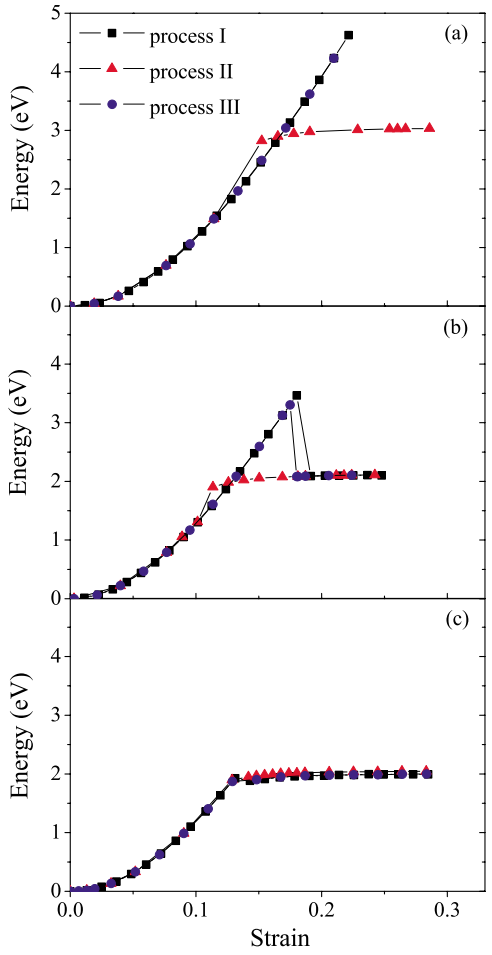


FIG. 2. (Color online) Total binding energy of the computation cell (in reference to the unstrained cell) as a function of strain applied by stretching processes I–III for the unit cell depicted in Fig. 1 with and without S. Panel (a) is for Ni GB without S, (b) for S at GB(0) site, and (c) for S at GB(2) site.

even though the charge density between GB(2) and GB(−2) atoms is higher than in the perfect crystal. The reduction in the GB(2)-GB(−2) bond length, nevertheless, has an important consequence when the system is under stress along the direction perpendicular to the GB (210) plane. As the system is stretched, the GB(3)-GB(−3) bond becomes even longer and weaker, whereas the GB(2)-GB(−2) bond will first be released to the perfect bulk value before it gets longer than that. Therefore, the GB(2)-GB(−2) bond will get stronger initially before it get too long so as to break. With this remedial, the chemical bonding across the GB plane is well comparable to that across a (210) plane inside the grain when stretched. Notice that in process II, at strain of 15%, the total binding energy of the unit cell is higher than in processes I and III. A similar deviation appears in the case for S at GB(0) [Fig. 2(b)]. At the first glance, it is tempting to attribute this deviation to numerical errors. But actually, this discrepancy is the consequence when the two grains are put too far away from each other (for a starting configuration) in stretching process II that an energy barrier appears which hinders the recombination of the two. Therefore, the system breaks at this strain even though the unbroken system (see the data points at the same strain in processes I and III) has a lower energy.

In the case that S segregates to GB(0) site [Figs. 2(b) and 3(b)], processes I and III did break the material. Although the GB has reflection symmetry along the stress direction, as in the clean GB case, the chemical bonding across the boundary plane is weaker than in the bulk environment [see Fig. 3(b)1]. Thus, small perturbations in stretching process I and III are able to break the symmetry and break the GB. Figure 2(b) shows that in both processes, an energy peak appeared before fracture occurred. We note that in order to get the exact UTS (maximum point), one has to use very dense tensile test points near the peak. The result that process III yielded a lower UTS than process I is conclusive as it is evident that in process III the system broke before it reached the maximum points in process I. On the other hand, process II, as in panel (a), did not show any peaks. It seems the calculated UTS is dependent to some extent on the stretching process. Our numerical results thus can serve as a strict assessment of the error incurred by insufficiency of simulation parameters.

It is noteworthy that since the total binding energy of the system drops to the same value immediately after it reaches the maximum for process I–III, these three stretching scheme predict the same Griffith energy.

In the case that S segregates to GB(2) site (panel c), stretching processes I–III yield essentially the same results. This is readily understandable based on our analysis made above. When the Ni atom at GB(2) site is replaced by S, GB(2), and GB(−2) sites are no longer symmetric. It is clearly seen in the top plot in Fig. 3(c) that the S atom bonds to Ni in the lower grain in a weaker manner than to the Ni atom in the upper grain. As a result, when stretched, the cell is broken, with S sticking to the upper grain, and there are no more metastable positions for GB core atoms in the stretching process.

To end this subsection, we want to address the sufficiency of thickness of the slab we have employed. Along the same way as we have done on the 21 layer slab, we have performed full computations on the clean and S-at-GB(0) GBs using 41 layer slabs. Here, the GB system was simulated by two connected grain each contains 21 atoms with one in common. In our previous study on vacancy segregation near the GB in nickel, we showed in the absence of external stress the 21 layer slab is able to yield a bulklike environment in the center of the Ni grain in the sense of multilayer relaxation near the GB (error bar ~0.01 Å) and formation energy (error bar ~0.01 eV) of the GB.[46] We used scheme I to stretch these two cells and obtained the total binding energies of them as a function of the strain yielded by applied stress (Fig. 4). Similar to Fig. 2, the stretching process I failed to break the clean GB at a strain as large as 20%, whereas it did break the GB with S atoms segregated GB(0) sites. In the latter case, the energy release during fracture is about 3.1 eV, approximately two times as large as the value for a 21 layer cell (1.5 eV). This is in accordance with the fact that at a given strain the elastic accumulation in the cell should be in proportion to its size. It is worth noting, however, the critical strain at which the system breaks is about 18% for the 21 layer cell but 15% for the 41 layer cell. This discrepancy

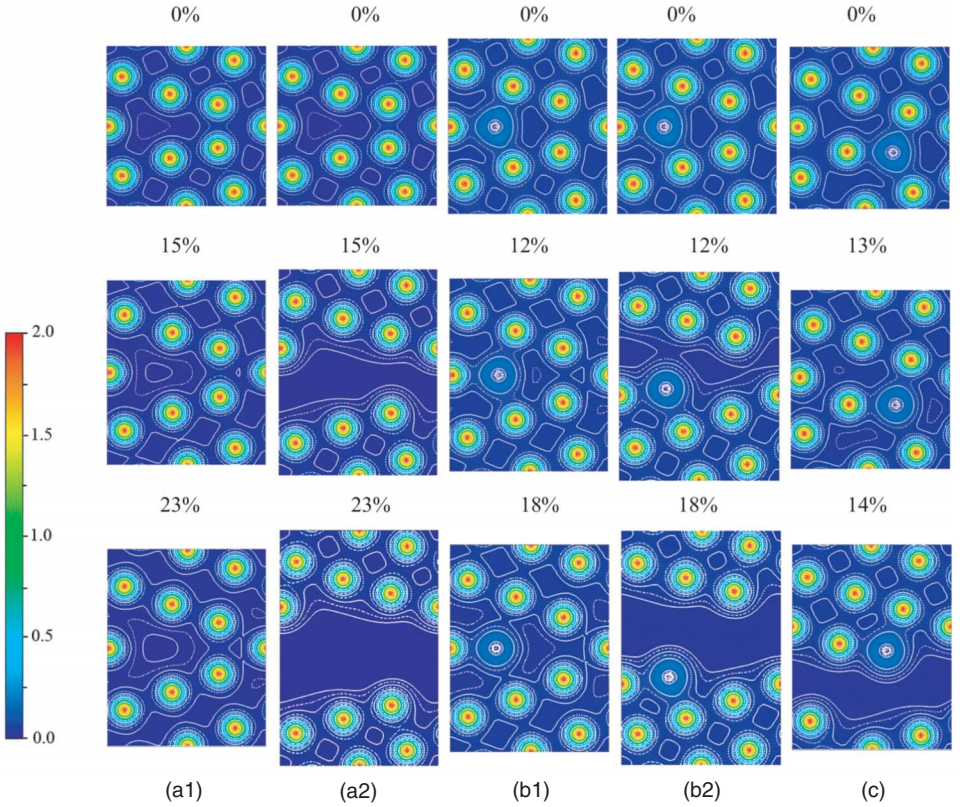


FIG. 3. (Color online) The calculated valence electron densities in the (001) plane near the Ni Σ5 (210) GB with and without segregated sulfur atoms, in the three stretching processes at different strains. Panels (a1) and (a2) are for the clean GB stretched in processes I and II at strains of 0%, 15%, and 23%; Panels (b1) and (b2) are for the GB with S at GB(0) site stretched in processes I and II at strains of 0%, 12% and 18%; and panel (c) is the GB with S at GB(2) stretched in Processes I, II, and III at strains of 0%, 13%, and 14%, respectively. The electron-density contours start from 0.03 $e/\text{a.u.}^3$ and increase successively by a factor of $10^{1/4}$.

comes from the fact that the GB and free-surface regions have different local elastic constant from the bulk. Our calculations show that for the clean GB system, the maximum strain, i.e., that strain at which the GB breaks is 2.94 Å for the 21 layer slab and 4.80 Å for the 41 layer slab. Clearly, at the break point, the added 20 layers which represent much better a bulk part contribute 1.86 Å. Based on this argument, the extrapolated maximum strain for a very thick slab will be 1.86 Å/20/0.79 Å=12%. Realizing this point, the absolute values of the maximum strain calculated for other systems should also be discussed only in a comparative manner, i.e., whether impurities enlarge or diminish it.

### B. Energy release: Metastable configurations

The occurrence of an energy release upon fracture, which contributes the UTS of the material, deserves further in-depth investigation. For a system with reflection symmetry along the stress direction, a configuration with reflection symmetry and the center layer of atoms staying at the center of the supercell is always at least a metastable state. When the load is large enough, it is no longer the ground state and is only metastable. An energy barrier appears between these two states and much extra tensile stress has to be applied in order to reach the broken configuration which has the lowest energy.

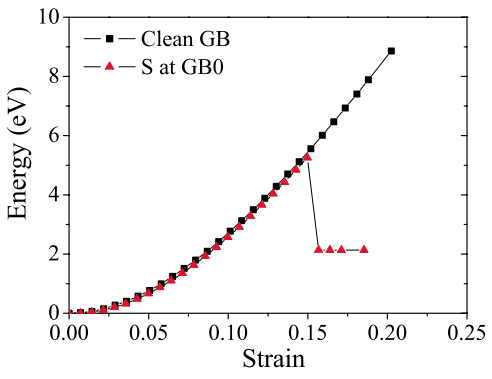


FIG. 4. (Color online) Total binding energy of the computation cell with 41 atomic layers as a function of strain applied by stretching processes I with and without S.

To see how sulfur decreases the energy release upon fracture, it is illustrating to trace the change in the above energy barrier along with the increase in the strain, for both the S-at-GB(0) and clean GB cases. For the former system, we have dealt with five configurations on the energy peak in process I [see Fig. 2(b)] with a strain of 14%, 15%, 16%, 17%, and 18%, respectively. For each configuration, we fixed the size of the unit cell and the position of the sulfur atom was also fixed at a series of distances away from the original (metastable) position. That is, S was relocated by hand to one side of the boundary to search the stable state without the reflection symmetry. We then allowed all the other atoms to relax and obtained the total energy. With this set of tedious calculations, we obtained the total energy as a function of the position of the S atom for each strain cases (Fig. 5) and thus are able to determine the energy barrier S encounters when it moves to the energetically favorable position. We see that the energy barrier is about 0.10 eV for the strain of 14%, and it decreases as the strain goes up. At the strain of 18%, it diminishes altogether, which means that the system can be broken by an infinitesimal perturbation.

As for the clean GB, we examined only one strain case (18%), in which the energy barrier has just appeared as the total energy exceeded the fractured configuration [see Fig.

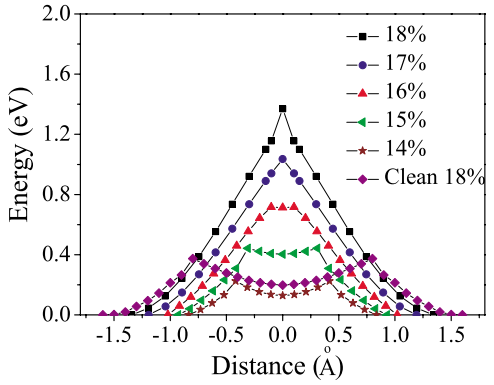


FIG. 5. (Color online) The calculated total binding energy (in reference to the ground state at a given strain) as a function of the position of the GB core atom when moving it by hand (and then fix) to one side of the computation cell. For the Ni Σ5 GB with S atom at GB(0) site, five strain cases (14%–18%) are presented. And for clean Ni Σ5 GB, only the case for a strain of 18% is investigated. The energy barrier between the metastable state with reflection symmetry and the ground state is clearly seen. Notice that the data corresponding to minus distances are obtained by simply mirroring the data for positive distances.

2(a) for the data point]. The total energy as a function of the position of the GB(1) Ni atom is shown as purple diamond in Fig. 5. The calculated energy barrier in this case is about 0.18 eV, remarkably larger than the S segregated case and much harder to break down. As discussed in Sec. III B, unlike the sulfur segregated case [see top plot in Fig. 2(b)1], the chemical bonding across the boundary plane in the clean GB case is well comparable to that across a (210) plane inside the grain [see top plots in Fig. 2(a)1]. Now we can understand why the clean GB has a higher-energy release than the one with segregated S and can therefore withhold higher tensile stress.

### C. Poisson effect

Until now, the lattice constants in the (210) plane were all fixed. That is, the Poisson effect was totally neglected. It is generally believed that neglecting the Poisson effect is acceptable as we often make comparative studies in the FPCTT on a GB with and without a segregated impurity. After all, taking into account the Poisson effect means that for each and every data point in Fig. 2, one has to perform at least four or five sets of full calculations in order to optimize the lateral lattice constants.

To put the FPCTT on a solid basis, it is now necessary to assess the influence of the Poisson effect on the calculated mechanical properties concerning GB cohesion. In doing so, we have carried out geometry optimization in the (210) plane for each and every data point in Fig. 2. Furthermore, we have also examined the possible variation in the $a$ to $b$ ratio in the (210) plane, for the clean GB case. In doing so, we optimized in turn $a$, $b$, $a$, $b$, and so on. For a strain of 8%, the optimized $a/b$ differs from the initial value within 1%, and the total energy is only 0.03 eV lower than the optimization with $a/b$ fixed. But for a strain as large as 25%, that is, in the nonlinear regime, we encountered a convergence problem. $a$ and $b$ started to oscillate after two rounds of optimization. This problem may be a sign for the Pulay stresses, and we will check and clarify this point in future investigation which involves more demanding computations. We suppose that relaxing $a/b$ will be a second-order effect compared to optimizing $ab$. A clarification of this point deserves further investigation.

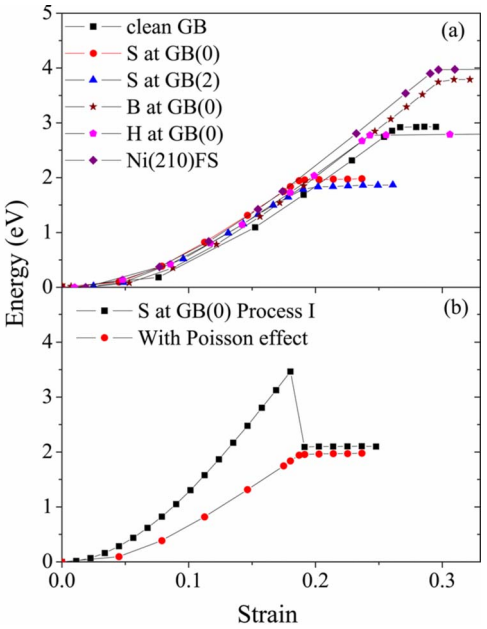


FIG. 6. (Color online) The calculated total binding energy of the unit cell depicted in Fig. 1 as a function of strain, in reference to the unstrained system. The Poisson effect has been taken into account. Also plotted is the result for a perfect crystal which is been stretched along the [210] direction. Note that the height of the platform of each curve represents the Griffith energy (toughness) of the corresponding system. In panel (b) we compare the results for S at GB (0) with and without consideration of the Poisson effect.

Figure 6 displays the calculated total binding energy of a unit cell as a function of applied strain with the consideration of the Poisson effect. To make easy comparison, we replot the result for elongation of the S-at-GB(0) system [Fig. 6(b)] using process I. The calculated Poisson ratio of these systems is about 0.30, very similar to the value for perfect Ni, 0.31.[47] Comparing with Fig. 2, we can see clearly that the Poisson effect reduces greatly the total energy of the system for intermediate strains. Those for the stress-free initial GB system and stress-free free surfaces (final state) systems are of course the same as before. Thus, the energy difference between the initial and eventual configurations is irrespective of the consideration of the Poisson effect. We note that for the clean GB, we still failed to separate the two grains in the unit cell by using the process I and III even with consideration of the Poisson effect, indicating that a clean Ni Σ5 GB is not a very weak point compared to the inner part of grains, and we have to disturb the GB core atoms by hand in order to break it. The result for the clean GB shown here is obtained by process II plus Poisson effect. But in the case that S segregates to GB(0) sites because the energy decrement induced by lateral contraction is larger than the energy re-

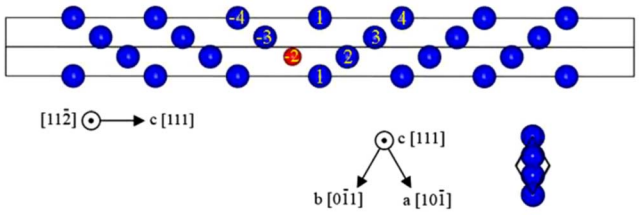


FIG. 7. (Color online) Side and top views of the computation cell used to model the Σ3 (111) [1$\bar{1}$0] tilt GB in Ni. Atoms near the GB are numbered by the atomic layer counted from the GB plane.

lease, energy peaks [see Fig. 2(b)] disappear, and we find no sudden energy release upon fracture. For convenience of comparison, we have also performed the FPCTT on a perfect Ni crystal along the [210] direction and on the effect of boron and hydrogen on the GB cohesion of Ni Σ5 (210). The numerical results demonstrate that boron is a strong cohesion enhancer; sulfur is a strong embrittler in both GB(2) and GB(0) sites; and hydrogen acts as a weak embrittler for this particular GB, in accordance with previous calculations[7] and experiment.[48]

Notice that since the lateral optimization of the lattice lowers the total energy of the system, the slope of the energy-versus-strain curve is reduced accordingly. As a result, the applied stress corresponding to each strain will be reduced too. Moreover, we want to note that the calculated maximum strain for the S-at-GB(2) system is greatly increased from 13% [see Fig. 2(c)] to 20% when the Poisson effect is taken into account. Since the energy difference between the initial and eventual configurations is unchanged, a prolonged maximum strain means a lesser sloped energy-versus-strain curve. Consequently, the theoretical tensile strength of this system will be significantly reduced.

### D. Ni Σ3 (111) [1$\bar{1}$0] GB

To make a comparative study and see the effect of lateral contraction on the energy release upon fracture for other type of GB, we have performed computations on Ni Σ3 (111) tile GB with a monolayer of sulfur atoms segregated to the GB(2) sites. In this set of computations, one unit cell contains two identical grains, each of which has nine atomic layers (see Fig. 7). The calculated interlayer distance between Ni (111) planes in the bulk is 2.03 Å. We have stretched the system using the processes I with and without the Poisson effect turned on.

We display in Fig. 8 the calculated total binding energy of the unit cell as a function of the strain. It is seen an energy peak of about 0.4 eV appears around strains of 6%. We note that in the Σ5 GB case, when sulfur segregated GB(2) site, there will be no such energy peak due to the loss of reflection symmetry in the stress direction. Moreover, the energy lowering induced by taking the Poisson effect into account is only marginal, in sharp contrast to the Σ5 case. This result can be readily understood if one recalls that in the Σ5 case, the crystal plane vertical to the stress direction is (210), which has a packing ratio of $\frac{\sqrt{5}\pi}{20} \cong 0.351$; whereas it is $\frac{\sqrt{3}\pi}{6} \cong 0.907$ for the (111) plane in the case of Σ3 (111) GB. Since

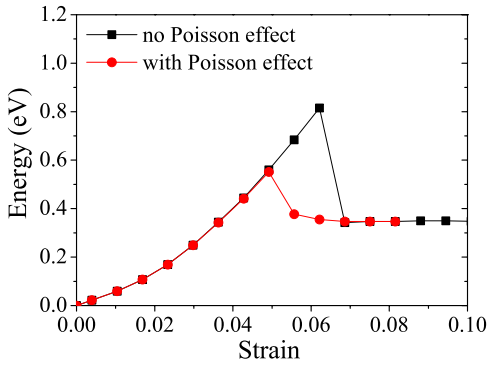


FIG. 8. (Color online) The calculated total binding energy of the computation cell containing a Ni Σ3 (111) GB with S segregate to the GB(2) site, as a function of strain applied by stretching process I, with and without the Poisson effect. Energies are in reference to the unstrained GB system.

atoms in the (111) plane are already closely packed, contraction will induce strong repulsion between Ni atoms which can easily overcompensate the energy gain by attractive interlayer interaction along the stress direction. And accordingly, lateral optimization of the lattice fails to get rid of the energy peak but only to reduce its magnitude.

To understand why there is a remarkable energy release at the breaking point for a nonsymmetric computation cell, we need to examine closely the electron densities around the sulfur atom at the GB. In Fig. 9 we can find that sulfur bonds to its neighboring Ni layers on left and right sides almost in the same manner although its bonding environment is not symmetric if next-nearest neighbors are taken into account. Such a balance makes this system comparable to the cases shown in Figs. 3(a) and 3(b), where energy release at the break point appears due to the reflection symmetry [with respect to the GB plane (210)] of the computation cell. Moreover, we can also see that sulfur bonds very slightly weaker with the GB core Ni than with the Ni layer on the other side (0%), and this tiny difference finally (3.5%-6.2%-7%) leads to the fracture occurring in between S and GB core layers.

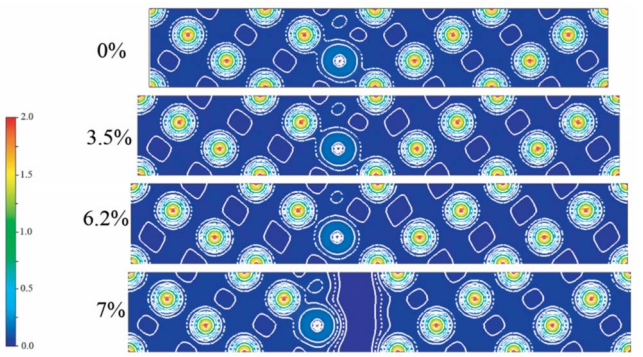


FIG. 9. (Color online) The calculated valence electron densities in the (1$\bar{1}$0) plane, near the Ni Σ3 (111) GB with S located at GB(2) site, in stretching process I. Charge density contours start from 0.01 $e$/a.u.$^3$ and increase successively by a factor of $10^{1/4}$. The strains are 0%, 3.5%, 6.2%, and 7%, respectively.

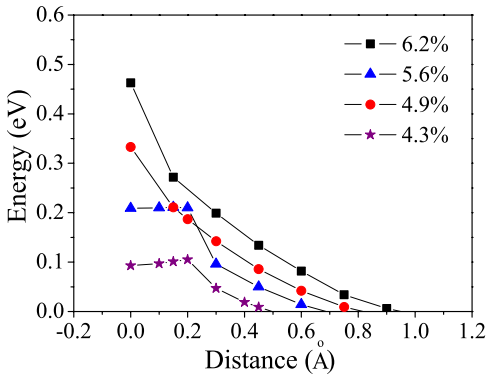


FIG. 10. (Color online) The calculated total binding energy (in reference to the ground state at a given strain) as a function of the position of the S atom when moving it by hand (and then fix) to one side of the computation cell. Four strain cases (4.2%, 4.9%, 5.6%, and 6.2%) are presented.

As we have done in the Σ5 (210) case, we now to trace the change in the energy barrier along with the increase in the strain in order to under the energy release upon fracture. Again, for each configuration, we fixed the size of the unit cell and the position of the sulfur atom was also fixed at a series of distances away from the original (metastable) position. That is, S was relocated by hand to the side of the boundary which it sticks to upon fracture. We then allowed all the other atoms to relax and obtained the total energy. Then we obtained the total energy as a function of the position of the S atom for each strain cases (Fig. 10) and thus are able to determine the energy barrier S encounters when it moves to the energetically favorable position. Interestingly, we see that the energy barrier is only about 0.01 eV for the strain of 4.2%, and it decreases down to zero as the strain goes up to 6.2%, where fracture occurs.

### E. Effect of magnetism

Although it is evident from Yamaguchi *et al.*'s study[49] that the bonding difference of sulfur to the Ni (210) free surface and to the Σ5 (210) GB changes only slightly with spin-polarization as a result of the weakness of Ni magnetism, there is still a great chance for the magnetism to influence the energy release upon fracture, as is shown in Secs. III A–III D that a minor change in the energy barrier between the metastable configuration and the true ground state at a given strain. With this in mind, we have restretched using process I the clean and S-at-GB(0) Ni Σ5 (210) GB in the presence of magnetism.

Figure 11 shows the calculated total binding energy of the computation cell as a function of the strain. In order to make comparison with nonmagnetic case easy, some results presented in Fig. 2 (denoted as NM) are shown here again. Clearly, for both clean and S segregated systems, effect of magnetism gets more remarkable with the increase in strain. For the clean Ni GB, the two grains are separated after the strain of 22% in spin-polarized calculation, whereas by the same tensile process (process I) we fail to break the nonmagnetic cell even with a strain as large as 30%. In the case that

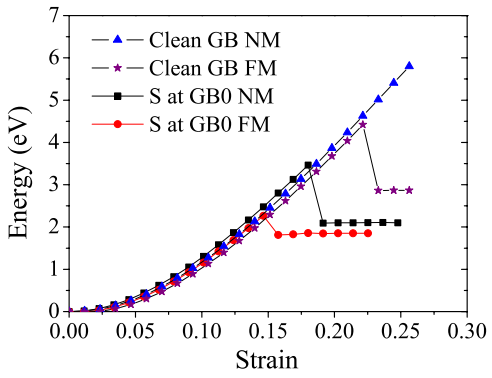


FIG. 11. (Color online) The calculated total binding energy of the computation cell as a function of strain applied by stretching process I, in reference to the energy of unstrained GB system. Also shown are the corresponding nonmagnetic results presented in Fig. 2

S segregated to GB(0) site, spin polarization reduces greatly the energy release from 1.5 to 0.5 eV. Although, the energy difference between the unstrained GB system (initial state) and the fractured system (final state with one free Ni surfaces, one absorbed with S) experiences a change in only 0.25 eV, the change in energy release upon fracture is as large as 1.0 eV. The finding that magnetism markedly reduces the toughness of the GB system was not expected from previous first-principles investigations.

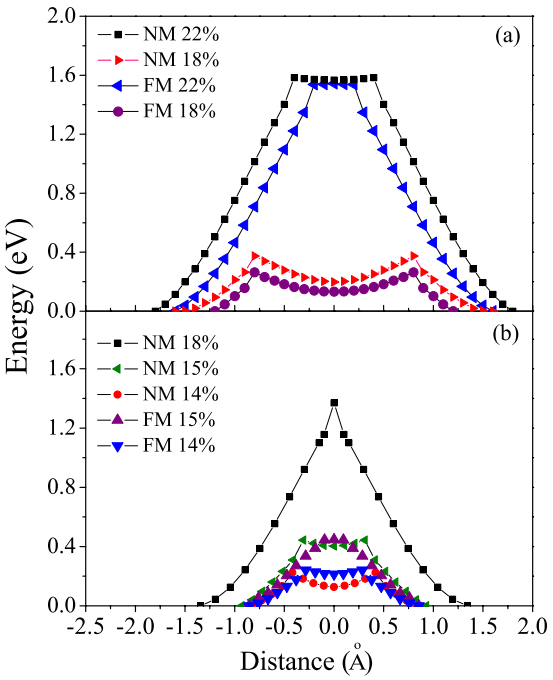


FIG. 12. (Color online) The calculated total energy (in reference to the ground state at a given strain) as a function of the position of the GB core Ni (panel a) or S (panel b) atom when moving it by hand (and then fix) to one side of the computation cell. A series of strain cases are presented. Both the nonmagnetic and magnetic results are presented. Panel (a) is for the clean Ni Σ5 GB and panel (b) is for S-at-GB(0) case. Same as in Fig. 5, the data corresponding to minus distances are obtained just by mirroring the data for positive distances.

The information of the energy barrier between the metastable state and the ground state while being stretched can be read from Fig. 12, which presents the total energy as a function of the position of the GB core Ni (panel a) or S (panel b) atom for each strain cases. In both cases, the energy barriers in FM states are smaller than those in the NM states at the same strain step. That is, magnetism reduces the energy barrier. Such an effect is more significant in the presence of sulfur. At the strain of 18%, FM state has an energy barrier about 0.05 eV lower than the NM state; while in the presence of S, it is about 0.07 eV lower at the strain of 14%. With a decreased energy barrier between the metastable configuration and the ground state, spin polarization cut down the energy releases at the break points.

As a final remark, we want to note that the limited physical size of our unit cell will lead to overestimating the tensile stress of the material due to the lack of dislocation nucleation. The periodic boundary conditions imposed in our first-principles density-functional theory computation will force the nickel grain boundary to become less ductile than in a polycrystalline form as no grain-boundary plasticity is allowed in such a simulation. Therefore, our conclusions regarding cohesive strength should be limited to being comparative only.

## IV. SUMMARY

To summarize, we have carried out a systematic investigation on the effect of lateral lattice optimization and spin polarization on the energy release upon fracture along Ni $\Sigma 5$ (210) and Ni $\Sigma 3$ (111) grain boundaries using FPCTT based on DFT. For the Ni $\Sigma 5$ (210) GB, the Poisson effect is significant in lowering the total energy of the system due to the openness of the (210) plane. Since the (111) plane is closely packed, lateral optimization of the computation cell has only a minor effect for the Ni $\Sigma 3$ (111) grain boundary. Magnetism is found to reduce much of the energy release upon fracture for grain boundaries, thereby diminishing the calculated ultimate tensile strength. Our results strongly suggest further investigations on materials such as Fe and its alloys with greater magnetism. It will shed light on what shall happen on the toughness in the loss of magnetism in Fe and steels.

## ACKNOWLEDGMENTS

This work was supported by the NSFC (Grant No. 50671011) and NCET (Grant No. 06-0080). The calculations were performed on the Quantum Materials Simulator of USTB.

*Corresponding author. geng@mater.ustb.edu.cn

[1] C. L. Briant and S. K. Banerji, in *Embrittlement of Engineering Alloys*, edited by C. L. Briant and S. K. Banerji (Academic Press, New York, 1983), p. 21.
[2] J. R. Rice and J. S. Wang, Mater. Sci. Eng., A **107**, 23 (1989).
[3] R. Wu, A. J. Freeman, and G. B. Olson, Science **265**, 376 (1994).
[4] R. Wu, A. J. Freeman, and G. B. Olson, Phys. Rev. B **53**, 7504 (1996).
[5] L. Zhong, R. Wu, A. J. Freeman, and G. B. Olson, Phys. Rev. B **55**, 11133 (1997).
[6] L. Zhong, R. Wu, A. J. Freeman, and G. B. Olson, Phys. Rev. B **62**, 13938 (2000).
[7] W. T. Geng, A. J. Freeman, R. Wu, C. B. Geller, and J. E. Raynolds, Phys. Rev. B **60**, 7149 (1999).
[8] W. T. Geng, A. J. Freeman, R. Wu, and G. B. Olson, Phys. Rev. B **62**, 6208 (2000).
[9] R. W. Smith, W. T. Geng, C. B. Geller, R. Wu, and A. J. Freeman, Scr. Mater. **43**, 957 (2000).
[10] J. X. Shang and C. Y. Wang, J. Phys.: Condens. Matter **13**, 9635 (2001).
[11] G. Lu, N. Kioussis, R. Wu, and M. Ciftan, Phys. Rev. B **59**, 891 (1999).
[12] W. T. Geng, A. J. Freeman, G. B. Olson, Y. Tateyama, and T. Ohno, Mater. Trans. **46**, 756 (2005) and references therein.
[13] W. T. Geng, A. J. Freeman, and G. B. Olson, Phys. Rev. B **63**, 165415 (2001).
[14] A. Y. Lozovoi, A. T. Paxton, and M. W. Finnis, Phys. Rev. B **74**, 155416 (2006).
[15] R. Schweinfest, A. T. Paxton, and M. W. Finnis, Nature (London) **432**, 1008 (2004).
[16] W. T. Geng, A. J. Freeman, and G. B. Olson, Mater. Trans. **47**, 2113 (2006).
[17] V. B. Deyirmenjian, V. Heine, M. C. Payne, V. Milman, R. M. Lynden-Bell, and M. W. Finnis, Phys. Rev. B **52**, 15191 (1995).
[18] M. Kohyama, Philos. Mag. Lett. **79**, 659 (1999).
[19] M. Kohyama, Phys. Rev. B **65**, 184107 (2002).
[20] G. H. Lu, S. Deng, T. Wang, M. Kohyama, and R. Yamamoto, Phys. Rev. B **69**, 134106 (2004).
[21] G. H. Lu, Y. Zhang, S. Deng, T. Wang, M. Kohyama, R. Yamamoto, F. Liu, K. Horikawa, and M. Kanno, Phys. Rev. B **73**, 224115 (2006).
[22] Y. Zhang, G. H. Lu, S. Deng, T. Wang, M. Kohyama, and R. Yamamoto, Mater. Trans. **47**, 2678 (2006).
[23] Y. Zhang, G. H. Lu, S. Deng, T. Wang, H. Xu, M. Kohyama, and R. Yamamoto, Phys. Rev. B **75**, 174101 (2007).
[24] C. G. Lee, X. D. Wei, J. W. Kysar, and J. Hone, Science **321**, 385 (2008).
[25] F. Liu, P. B. Ming, and J. Li, Phys. Rev. B **76**, 064120 (2007).
[26] R. Khare, S. L. Mielke, J. T. Paci, S. L. Zhang, R. Ballarini, G. C. Schatz, and T. Belytschko, Phys. Rev. B **75**, 075412 (2007).
[27] Note that if only initial and eventual configurations are to be examined, FPCTT reduces to FPRW method.
[28] H. Van Swygenhoven and P. M. Derlet, Phys. Rev. B **64**, 224105 (2001).
[29] D. Farkas, H. Van Swygenhoven, and P. M. Derlet, Phys. Rev. B **66**, 060101 (2002).
[30] H. Van Swygenhoven, Science **296**, 66 (2002).
[31] A. Hasnaoui, H. Van Swygenhoven, and P. M. Derlet, Science **300**, 1550 (2003).
[32] Z. Budrovic, H. Van Swygenhoven, P. M. Derlet, S. V. Petegem, and B. Schmitt, Science **304**, 273 (2004).

[33] A. J. Cao and Y. G. Wei, Phys. Rev. B **76**, 024113 (2007).
[34] M. Yamaguchi, M. Shiga, and H. Kaburaki, Science **307**, 393 (2005).
[35] W. T. Geng, J. S. Wang, and G. B. Olson, Science **309**, 1677c (2005).
[36] M. Yamaguchi, M. Shiga, and H. Kaburaki, Science **309**, 1677d (2005).
[37] D. L. Adams, L. E. Petersen, and C. S. Sorensen, J. Phys. C **18**, 1753 (1985).
[38] A. J. Freeman and R. Wu, J. Magn. Magn. Mater. **100**, 497 (1991) and references therein.
[39] W. T. Geng, A. J. Freeman, and R. Q. Wu, Phys. Rev. B **63**, 064427 (2001).
[40] G. Kresse and J. Furthmuller, Comput. Mater. Sci. **6**, 15 (1996); G. Kresse and J. Furthmuller, Phys. Rev. B **54**, 11169 (1996).
[41] P. E. Blochl, Phys. Rev. B **50**, 17953 (1994).
[42] G. Kresse and D. Joubert, Phys. Rev. B **59**, 1758 (1999).
[43] J. P. Perdew, K. Burke, and M. Ernzerhof, Phys. Rev. Lett. **77**, 3865 (1996).
[44] J. K. Heuer, P. R. Okamoto, N. Q. Lam, and J. F. Stubbins, J. Nucl. Mater. **301**, 129 (2002).
[45] T. Shinoda and T. Nakamura, Acta Metall. **29**, 1631 (1981).
[46] W. Xiao, C. S. Liu, Z. X. Tian, and W. T. Geng, J. Appl. Phys. **104**, 053519 (2008).
[47] A. S. M. Metals Handbook, *Properties and Selection: Nonferrous Alloys and Pure Metals* (American Society for Metals, Metals Park, OH, 1979), Vol. 2.
[48] R. H. Stulen, *Proceeding of the Second JIM International Symposium on Hydrogen in Metals*, Supplement to Trans. Jpn. Inst. Met., **21**, 501 (1980).
[49] M. Yamaguchi, M. Shiga, and H. Kaburaki, Mater. Trans. **47**, 2682 (2006).